

## Cell dynamical system approach to block copolymers

M. Bahiana and Y. Oono

*Department of Physics, Materials Research Laboratory and Beckman Institute,  
1110 West Green Street, University of Illinois at Urbana-Champaign, Urbana, Illinois 61801*

(Received 5 February 1990)

A cell-dynamical-system (CDS) model of the microphase separation of block copolymers is described in detail. The model suggests a partial-differential-equation (PDE) model that allows us to find a close relation between the block copolymer and spinodal decomposition problems. A detailed numerical study of the CDS model is given, which indicates that hydrodynamic effects are crucial for very late time-ordering processes. The strong segregation regime is studied analytically with the aid of an exactly solvable PDE model, which is suggested by the universality supported by the CDS simulations. The results obtained show that dimensional analysis gives the correct exponent for the block copolymer lamellar thickness.

### I. INTRODUCTION

A diblock copolymer (BCP) is a linear-chain molecule consisting of two subchains  $a$  and  $b$  grafted covalently to each other [Fig. 1(a)]. The subchains  $a$  and  $b$  are made of different monomer units  $A$  and  $B$ , respectively. In polymer systems even a weak repulsion between unlike monomers  $A$  and  $B$  induces a strong repulsion between  $a$  and  $b$ . As a result, the different subchains tend to segregate below some temperature  $T_c$ , but, as they are chemically bonded, even a complete segregation of subchains  $a$  and  $b$  cannot lead to a macroscopic phase separation as in mixtures of two homopolymers. Only a local microphase separation occurs: microdomains rich in  $A$  or  $B$  are formed [see Fig. 1(c)]. These ordered structures are the key to many valuable mechanical properties which make block copolymers of great technological interest. Besides its practical importance, the BCP microphase separation is an interesting problem in itself, because it allows the

possibility of studying a phase transition from a spatially uniform state to a nonuniform state which can be controlled by, for example, chemically modifying monomers.

The main purpose of this paper is threefold. First, we explain the discrete space-time mesoscale (kinetic level) model of the BCP melt in terms of cell dynamical systems (CDS's), which are computationally efficient discrete space-time models,<sup>1-3</sup> and have been successfully applied to other phase-ordering problems.<sup>4-11</sup> Originally, we thought<sup>5</sup> our approach was essentially an alternative derivation of the mesoscale model due to Leibler,<sup>12</sup> but we have found that there is a crucial difference in the coarse-graining length scale. Our CDS model was devised by pursuing mathematical simplicity. We find that our model is more physical than the model derived from the purportedly microscopic description of the system. Second, detailed computational results obtained with the aid of the CDS model are given. Comparison of patterns obtained in actual systems and our computation demonstrates that hydrodynamic effects are crucial for very late time-ordering processes. We also summarize a close connection between spinodal decomposition and the BCP microphase separation.<sup>13</sup> Third, detailed results obtained from an exactly solvable model<sup>14</sup> are presented.

A brief summary of some experimental and theoretical results directly relevant to our work is given in Sec. II. In Sec. III, we model the BCP system in terms of cell dynamical systems (CDS's). Section IV describes our computational results. The effect of hydrodynamics is discussed here briefly. Even with our efficient model we were unable to go into the so-called strongly segregated regime, but we could verify a scaling hypothesis at least in the weak segregation regime. In Sec. V, we point out a close relation between the BCP problem and spinodal decomposition. Dimensional analysis gives us the correct exponent for the layer thickness in terms of the molecular weight. In Sec. VI, the strong segregation regime is studied with the aid of an exactly solvable model. Section VII is a discussion.

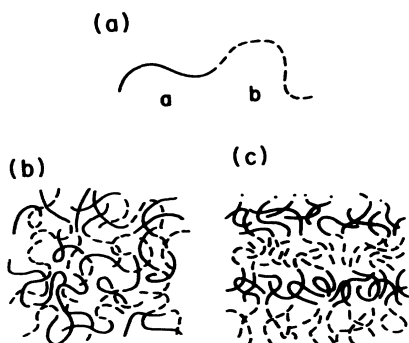


FIG. 1. (a) A diblock copolymer molecule. We consider here only the 1:1 block copolymer which has equal sized subchains  $a$  and  $b$ . (b) Above  $T_c$ ,  $a$  and  $b$  subchains mix to make a uniform disordered phase. (c) Below  $T_c$  the subchains  $a$  and  $b$  tend to segregate, but due to the covalent bonds between the subchains, segregation is possible only locally to form a lamellar structure.

## II. BRIEF SUMMARY OF EXISTING RESULTS

Depending on the ratio of the block sizes and on the solvent, different mesoscale structures are observed.<sup>15–18</sup> For a BCP in which the length of the subchains are roughly the same (even BCP), a lamellar structure is observed. The ratio of the interfacial and the lamellar thicknesses characterizes the segregation regime. If the temperature is not very different from the critical temperature  $T_c$ , that is, if the quenching is shallow, the interfacial thickness  $\xi$  is comparable to the equilibrium lamellar thickness  $D$ . This regime is called the weak segregation (WS) regime. If the quench is sufficiently deep, then  $\xi \ll D$  and the system is said to be in the strong segregation (SS) regime. Hashimoto, Shibayama, and Kawai<sup>19</sup> have studied the dependence of  $D$  on the polymerization index  $N$  for copolymers with lamellar structures. They have found that  $D \sim N^\theta$ , with the value of  $\theta$  depending on the segregation regime. In the WS regime  $\theta = \frac{1}{2}$ , and in the SS regime  $\theta = \frac{2}{3}$ . They have found that  $\xi$  is almost independent of the number-averaged molecular weight  $M_n$  within the range  $21 \times 10^3$  to  $102 \times 10^3$ . As a consequence, the volume fraction of the interfacial region systematically decreases with increasing molecular weight.

The first important theory of block copolymer microdomain structure was presented by Meier,<sup>20</sup> who considered spherical domains using random-flight statistics. He found that the radius of the domains scales as  $N^{1/2}$  and that the domains have greater density at the boundary. Helfand and Wasserman<sup>21–24</sup> developed a microscopic theory in the SS regime based on the random-walk model. They obtained the free energy in terms of the lamellar thickness. Minimization of this free energy gave  $D \sim N^{0.643}$  numerically.

Leibler<sup>12</sup> devised the first mesoscopic theory. He derived the free-energy functional for BCP in terms of the order parameter  $\psi(\mathbf{r})$  defined as the local concentration difference of monomers  $A$  and  $B$ . He studied the WS regime with this free energy and found that  $D \sim N^{1/2}$ . Ohta and Kawasaki<sup>25</sup> studied the SS regime with a variational approach, using the Leibler effective free-energy functional. They obtained the SS exponent, that is,  $D \sim N^{2/3}$ . Later, they<sup>26</sup> generalized their derivation of the free-energy functional beyond the random-phase approximation, and confirmed their conclusion. Recently, Liu and Goldenfeld<sup>27</sup> numerically determined the free energy as a function of the lamellar thickness for the Leibler model to obtain both SS and WS exponents.

When the lengths of the subchains  $a$  and  $b$  are not equal (uneven BCP), various mesoscale structures are observed.<sup>15–18</sup> They are also theoretically studied in Refs. 21–25. We will not consider these cases in this paper nor will we discuss the role of the solvent in the microphase separation.<sup>28</sup> We assume that chains are sufficiently flexible, so we will not discuss the stiffness effect.<sup>29</sup>

## III. A CELL-DYNAMICAL-SYSTEM MODEL

The cell-dynamical-system model for block copolymers proposed by Oono and Shiwa<sup>5</sup> is based on the CDS model for binary alloy spinodal decomposition by Oono and

Puri.<sup>1–3</sup> In the latter case the general form of the CDS for the order parameter  $\psi$  in each cell reads

$$\psi(t+1, n) = \psi(t, n) + \mathcal{J}(t, n) - \langle \langle \mathcal{J}(t, n) \rangle \rangle, \quad (3.1)$$

with

$$\mathcal{J}(t, n) \equiv f(\psi(t, n)) + \mathcal{D}[\langle \langle \psi(t, n) \rangle \rangle - \psi(t, n)] - \psi(t, n), \quad (3.2)$$

where  $\psi(t, n)$  is the order parameter in the  $n$ th cell at time  $t$ ,  $\mathcal{D}$  is a positive constant proportional to the diffusion constant, and  $\langle \langle \rangle \rangle$  is the isotropic spatial average. For a two-dimensional (2D) square lattice, we choose

$$\langle \langle \psi(t, n) \rangle \rangle = \frac{1}{6} \sum_{\mathcal{N}} (\psi_{\mathcal{N}}) + \frac{1}{12} \sum_{\mathcal{N}\mathcal{N}} (\psi_{\mathcal{N}\mathcal{N}}), \quad (3.3)$$

where  $\mathcal{N}$  represents nearest-neighbor cells and  $\mathcal{N}\mathcal{N}$  represents next-nearest-neighbor cells. The map  $f$  has a flow with a single hyperbolic unstable fixed point and two hyperbolic stable fixed points symmetrically located on each side of the unstable fixed point. The exact form of  $f$  is not important for the late-stage behavior, as was demonstrated in Ref. 1. We will later exploit this universality to construct a solvable model. Here  $f(\psi) = A \tanh[\psi(t, n)]$  has been chosen. Above the critical temperature  $A < 1$ , and below  $A > 1$ . The usefulness of the scheme has been well demonstrated by various applications,<sup>2–11</sup> etc. Strictly speaking, the current numerical solutions of partial-differential-equation (PDE) models [in this case the Cahn-Hilliard (CH) equation, e.g., Ref. 30] should be considered as CDS simulations, because the adopted numerical schemes are too crude to get the actual long-term solutions to the PDE.

To construct a CDS model of BCP, our strategy is to find the minimum modification of the above CDS model for spinodal decomposition. In ordinary spinodal decomposition the domain size increases indefinitely. In contrast, the domain growth of BCP is limited by the covalent bond between subchains  $a$  and  $b$ . In other words, the state with  $\psi=0$  becomes more stable than that with  $\psi \neq 0$  when there is no spatial gradient. The simplest way to take this into account is to modify (3.1) as follows:

$$\psi(t+1, n) = (1-B)\psi(t, n) + \mathcal{J}(n, t) - \langle \langle \mathcal{J}(n, t) \rangle \rangle, \quad (3.4)$$

where  $B$  is a small positive number. In a large bulk cluster,  $\psi$  is spatially uniform so that  $\mathcal{J}$  and its local average  $\langle \langle \mathcal{J} \rangle \rangle$  become identical. Hence, in the bulk phase (3.4) simply reads  $\psi(t+1, n) = (1-B)\psi(t, n)$ , which has the fixed point at  $\psi=0$ . We could add thermal noise, but the noise effect is not crucial as we will see below (see also Ref. 31).

In the above construction of the model, there is an important implicit assumption that the local free energy which drives the segregation of monomers is not affected by the global chain connectedness (or the molecular weight). We believe this is physically sound, because for local segregation dynamics the effect of the total length of the chain is extremely indirect. Hence, even the length ratio of the subchains should not appear in the local part

of the free energy. Furthermore, the local dynamics should not reflect the molecular weight of the chain, because in our modeling each cell is considered to be considerably smaller than the polymer size. In other words, our CDS model has a coarse-grain scale finer than the correlation length in the system. Hence, our model parameters  $A$  and  $\mathcal{D}$  should not depend on the molecular weight or the composition. Notice that this point is diametrically different from the conventional mesoscale models summarized in Sec. II. We feel that these models are over coarse grained, if their derivation is justifiable mathematically. This difficulty seems to be well recognized by Kawasaki and Ohta.<sup>22</sup> Leibler's method is the same as that used by Edwards in his theory of polymer melt.<sup>33</sup> It has been amply demonstrated that the method is quantitative in semidilute solutions,<sup>4</sup> but for denser systems its mathematical soundness should be seriously questioned. We are interested only in the long-time behavior of the system, so that the detailed mechanism of diffusion is unimportant.

The partial differential equation corresponding to (3.4) can be obtained if we trace in reverse the derivation of PDE from the CDS given in Refs. 1 and 3. The result for the BCP with equal size subchains is

$$\frac{\partial \psi}{\partial t} = \Delta(-\tau\psi + u\psi^3 - \mathcal{D}\Delta\psi) - B\psi, \quad (3.5)$$

which is essentially the Cahn-Hilliard equation<sup>35</sup> with the subtraction of  $B\psi$ .  $\tau$ ,  $u$ , and  $\mathcal{D}$  are positive phenomenological parameters,  $\tau$  being a measure of the quench depth, and  $\Delta$  is the Laplacian. Equation (3.5) can be rewritten as

$$\frac{\partial \psi}{\partial t} = \Delta \left[ -\tau\psi + u\psi^3 - \mathcal{D}\Delta\psi + B \int d\mathbf{r}' G(\mathbf{r}, \mathbf{r}') \psi(\mathbf{r}', t) \right], \quad (3.6)$$

where  $G$  is the Green's function for Laplace's equation  $\Delta G(\mathbf{r}, \mathbf{r}') = -\delta(\mathbf{r} - \mathbf{r}')$ , under a suitable boundary condition. If the above equation is rewritten as the ordinary CH equation

$$\frac{\partial \psi}{\partial t} = \Delta \frac{\delta H}{\delta \psi}, \quad (3.7)$$

then the Hamiltonian  $H$  has a similar form as the one derived by Leibler<sup>12</sup> with  $B \propto N^{-2}$ . As is discussed above, however, contrary to our interpretation in our previous papers, the similarity is *not* straightforward, and could even be fortuitous. The identification  $B \propto N^{-2}$  is still justifiable dimension-analytically as is already mentioned in Ref. 13. We do not discuss the problem of microscopic computation of phenomenological parameters. This should be much more complicated than was thought by previous authors. It is fair to say that even for PDE models we do not know how to compute phenomenological constants. This comments also applies to the even simpler CH equation.

#### IV. COMPUTATIONAL RESULTS

Our simulations were performed on a CRAY X-MP computer with  $A = 1.3$ ,  $\mathcal{D} = 0.5$  with random initial con-

ditions of an amplitude 0.05 and a periodic boundary condition, unless otherwise stated in the figure captions. Figure 2 exhibits the patterns obtained from (4.1) for a  $200 \times 200$  square lattice at different times. For uneven BCP, the necessary minimal modification is to stabilize an appropriate local concentration compatible with the subchain size ratio. Let  $r$  be the ratio of the length of the shorter subchain and the total chain length. In this case we should stabilize  $\psi = 2r - 1$  instead of  $\psi = 0$ , so that we obtain

$$\psi(t+1, n) = \psi(t, n) - B[\psi(t, n) - 1 + 2r] + \mathcal{J}(t, n) - \langle \mathcal{J}(t, n) \rangle. \quad (4.1)$$

The pattern resulting from this modification can be seen in Fig. 3.

As discussed in Sec. III, there seems to be no really reliable derivation of the mesoscale model in this case, so we used this minimal model for the uneven cases. Here we have assumed that the molar volume ratio is identifiable with the subchain length ratio for simplicity. The choice  $B = 0$  recovers the ordinary spinodal decomposition.

The patterns above are remarkably similar to the real ones observed in thin film experiments by Douy and Gallot<sup>18</sup> and Kämfer, Hoffman, and Krömer.<sup>17</sup> Patterns observed in cross sections of thicker films though, are quite different from Fig. 2. They present a well-defined lamellar structure in which the layers are mostly parallel to the film surface.

In order to explain this difference, we have suggested the relevance of spatial dimensionality,<sup>13</sup> because the interface of the 2D scalar model is always rough<sup>36,37</sup> in contrast to the 3D counterpart.<sup>38</sup> However, simulations on a

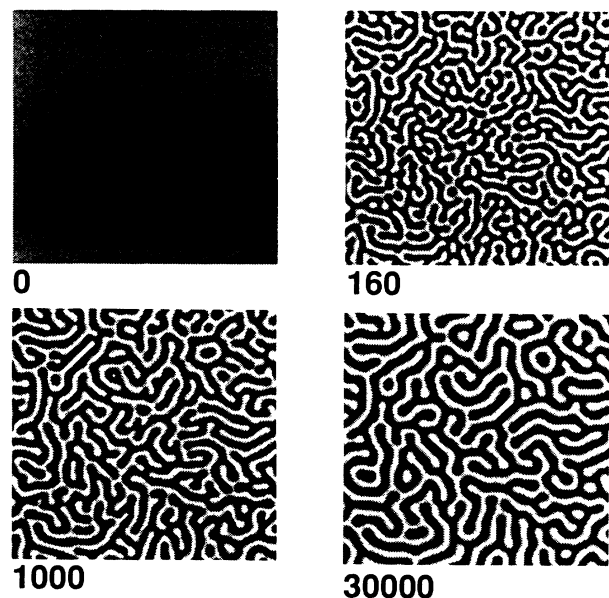


FIG. 2.  $200 \times 200$  patterns with  $A = 1.3$ ,  $\mathcal{D} = 0.5$ ,  $B = 0.005$ ,  $r = \frac{1}{2}$ . The numbers denote time steps. The pattern does not change significantly after about 10 000 steps.

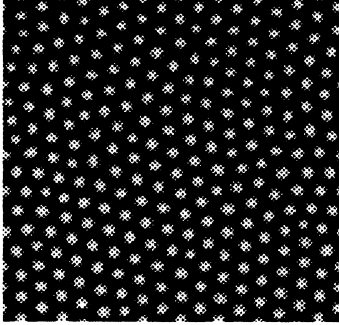


FIG. 3.  $128 \times 128$  pattern after 30 000 iterations with  $A = 1.3$ ,  $\mathcal{D} = 0.5$ ,  $B = 0.02$ , and  $r = 0.4$ .

3D system demonstrate that this is not the case; the cross-sectional pattern in Fig. 4 have the same characteristics as the 2D patterns. One might suggest that the result is not surprising, because our model is deterministic, but, as we see from Fig. 5, the addition of sufficiently large thermal noise brings nothing new.

Rabin<sup>39</sup> argues that since the molecules in our system are large, there should be a penalty for interface bending just as in the case of micelles. It is not difficult to incorporate a penalty for a small radius of curvature of the interface; we add a double Laplacian term to the free energy as

$$\mathcal{J}'(t, n) \equiv f(\psi(t, n)) - \psi(t, n) + \mathcal{D}[\tilde{\Delta}\psi(t, n) - b\tilde{\Delta}^2\psi(t, n)], \quad (4.2)$$

where  $\tilde{\Delta}$  is the discrete Laplacian:  $\tilde{\Delta} \cdots \equiv \langle\langle \cdots \rangle\rangle - \cdots$  and  $b > 0$ . A pattern obtained with this scheme can be seen in Fig. 6. Of course, domains try to avoid configurations with small radii of curvature, so that the pattern is locally ordered, but still no long-range lamellar structure is observed. Thus we may conclude that the suggested special property of the interface is not significant in our system.

Suppose that we have obtained a pattern with parallel but meandering lamellae. To straighten lamellae, many polymer chains must be removed from positive curvature interface portions. With the diffusion mechanism only, this becomes prohibitively difficult after microdomains are established. We need a mechanism to move polymer chains perpendicular to the layer. The simplest realistic mechanism is a flow which translates lamellae perpendic-



FIG. 4. Cross section of a 3D system with the lattice size  $100 \times 100 \times 50$  with  $A = 1.3$ ,  $\mathcal{D} = 0.5$ , and  $B = 0.02$  at  $t = 1000$ .

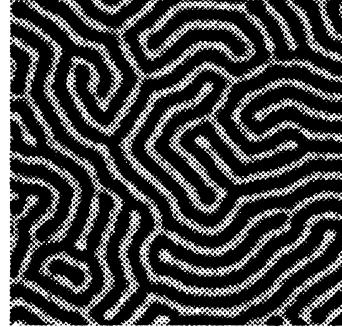


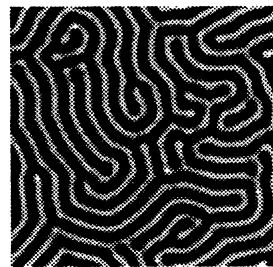
FIG. 5. Pattern after 30 000 steps obtained from (3.4) with noise added in the following way:

$$\begin{aligned} \psi(t+1, n) = & (1-B)\psi(t, n) + \mathcal{J}(n, t) - \langle\langle \mathcal{J}(n, t) \rangle\rangle \\ & + C[\eta_x(t, n_x+1, n_y) - \eta_x(t, n_x, n_y) \\ & + \eta_y(t, n_x, n_y+1) - \eta_y(t, n_x, n_y)]. \end{aligned}$$

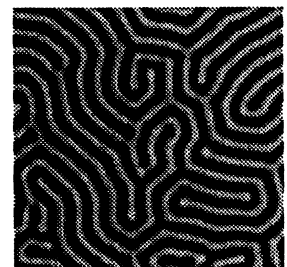
Here, the lattice size is  $128 \times 128$ ,  $B = 0.02$ , and noise amplitude  $C = 0.05$ .

ular to the interface. The spatially nonuniform distribution of chemical potential establishes global flow in the system, which can gradually distort global patterns. The dynamics of BCP with a hydrodynamic effect will be discussed in a separate paper, but a prototypical demonstration in Fig. 7 and 8 clearly shows the importance of hydrodynamic effects. Here a thin layer of BCP melt is sandwiched between two plates, i.e., is placed in a Hele-Shaw cell. For the formation of layers it is also crucial to have a suitable boundary condition as can be seen there. Experimental conditions under which well-ordered lamellar structures are formed seem to always have some kind of fluidity and a substrate.

Although without hydrodynamics we cannot get a well-ordered lamellar structure, the evolution of the lamellar thickness is determined by local dynamics.



(a)



(b)

FIG. 6. Effect of the penalty for the interface bending after 30 000 timesteps. The patterns are  $128 \times 128$  and have  $A = 1.3$ ,  $\mathcal{D} = 0.45$ , and  $B = 0.02$ . In (a)  $b = 0$ , that is, no penalty. In (b)  $b = 1.1$ . Both patterns were obtained starting from the same initial condition.

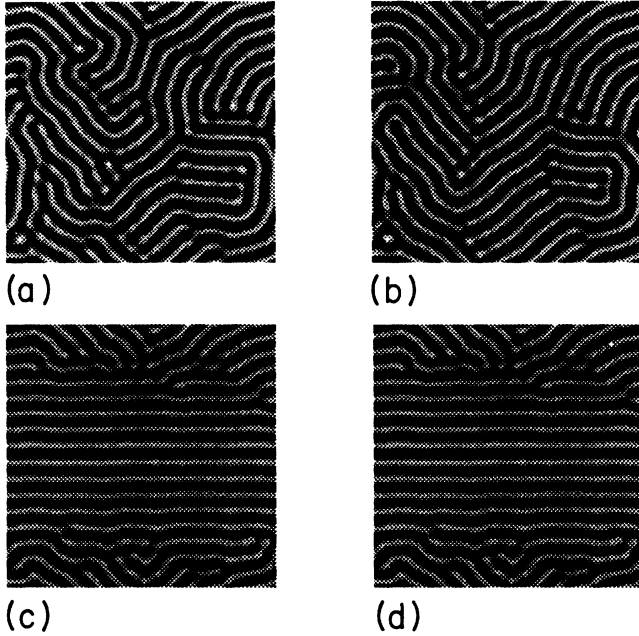


FIG. 7. Effect of the boundary conditions in the formation of lamella. Patterns on the left correspond to 10 000 iterations, and on the right, 30 000. Here,  $A=1.22$  and  $B=0.02$ . (a) and (b) have periodic boundary conditions in both directions; (c) and (d) have the central line fixed at  $\psi=0.5$ . The introduction of a fixed boundary condition has promoted some ordering, but the evolution of the pattern after 10 000 iterations is extremely slow. Layers with large component parallel to ordering direction are almost frozen.

Therefore, we may still use our model (3.4). Examining the cross sections for patterns at  $t=9000$  time steps for  $B=0.0008$ , we see that the interface is still with the same order of magnitude as the domain size, indicating that the system is in the weak segregation regime. Simulations for smaller values of  $B$  are difficult due to finite size effect even in  $500 \times 500$  lattices.

To study the dependence of the equilibrium pattern size on  $B$ , we computed the static form factor  $S(\mathbf{k})$ , defined as  $S(\mathbf{k}) \equiv \langle \psi_{\mathbf{k}} \psi_{-\mathbf{k}} \rangle$  with  $\psi_{\mathbf{k}}$  being the Fourier transform of the order parameter, after sufficiently long time. The average  $\langle k \rangle$  of  $|\mathbf{k}|$  is defined as

$$\langle k \rangle \equiv \int_0^\infty dk k S(k) / \int_0^\infty dk S(k), \quad (4.3)$$

where  $S(k)$  is the spherically averaged  $S(\mathbf{k})$ . Regarding  $\langle k \rangle^{-1}$  as a measure of the lamellar thickness  $D$ , we find  $D \sim B^\alpha$  with  $\alpha = -0.256 \pm 0.003$  (see Fig. 9).<sup>13</sup>

## V. EXPONENTS AND SCALING

The equilibrium pattern should obey

$$B\psi = \Delta(-\tau\psi + u\psi^3 - \mathcal{D}\Delta)\psi. \quad (5.1)$$

Comparing this result with the CH equation [(3.5) with  $B=0$ ], we realize that dimension analytically [ $B^{-1}$ ] corresponds to  $[t]$ , i.e.,  $[N^2]$  corresponds to  $[t]$  (square

brackets denote standard notation). Hence the asymptotic growth law  $l(t) \sim t^\phi$  for the CH equation, which is usually the dimension-analytic result,<sup>40</sup> should imply  $l \sim N^{2\phi}$ , that is,  $\theta=2\phi$ . Notice that (5.1) has infinitely many solutions, but the one with the lowest free energy should have well-defined thin interfaces for sufficiently small  $B$ .

The results above suggest the following scaling hy-

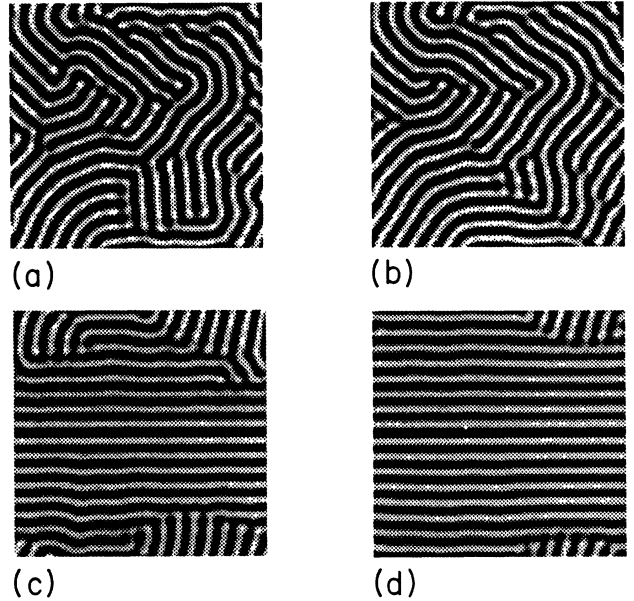


FIG. 8. Effect of hydrodynamic interactions in the formation of lamellar patterns, in a Hele-Shaw cell. To incorporate global flow in our model, we followed Shinozaki and Oono (Ref. 11). A term corresponding to the fluid motion was added to (3.5). Assuming the incompressibility condition for the velocity field  $\nabla \cdot \mathbf{v} = 0$  the resulting equation is  $\partial\psi/\partial t = \Delta(\delta H/\delta\psi) - \mathbf{v} \cdot \nabla\psi$ .  $\mathbf{v}$  can be calculated starting from the Navier-Stokes equation with the introduction of the following approximations: (i) the fluid is considered to be in the Stokes regime; (ii) the velocity field is slaved to the slower process of phase separation; (iii) the distance between the planes in the Hele-Shaw cell is much smaller than the domain size, so that we can eliminate  $\Delta$  in favor of a geometric factor  $-c^2$ , which is roughly the inverse of the interplate distance squared. With these we get  $\mathbf{v} = -1/c^2 \nu [\nabla p + \psi \nabla(\delta H/\delta\psi)]$ , where  $p$  is the pressure and  $\nu$  the kinematic viscosity.  $-\psi \nabla \delta H/\delta\psi$  is a force density felt by the fluid due to the existence of a chemical “pressure”  $\delta H/\delta\psi$ . The incompressibility constraint allows us to compute the pressure, and hence the velocity field. A  $128 \times 128$  lattice is used with  $A=1.22$ ,  $\mathcal{D}=0.45$ ,  $\nu c^2=2.0$ ,  $B=0.02$ . The patterns on the left correspond to 10 000 timesteps, and on the right, 30 000. The systems in (a) and (b) have periodic boundary conditions in both directions. (c) and (d) have the central line fixed at  $\psi=0.5$ . We can see that the fixed boundary condition is essential for obtaining a well structured lamellar pattern. The ordered lamella are formed from domains oriented perpendicularly to the fixed surface, a condition that appears only when flow is added to the simulation (compare with Fig. 7). Also it is important to notice that although the equilibrium lamellar size is well established before  $t=5000$  time steps for this value of  $B$ ; only after 30 000 iterations is the ordered pattern obtained.

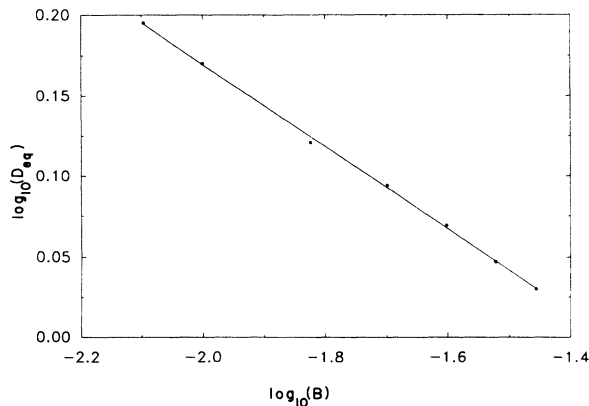


FIG. 9. Empirical relation between the lamellar thickness  $D$  and  $B$ . The solid line is the least squares fitting with a slope of 0.256 corresponding to  $\theta=0.5$ , which indicates that the system is in the WS regime.  $D$  represents the average over 30  $100 \times 100$  systems.

pothesis for the domain size:

$$D(t, B) = B^\alpha F(tB), \quad (5.2)$$

where  $F(x)$  is independent of  $B$ . Figure 10 shows the result of plotting our data according to this scaling hypothesis. We see that indeed the relation (5.2) is verified.

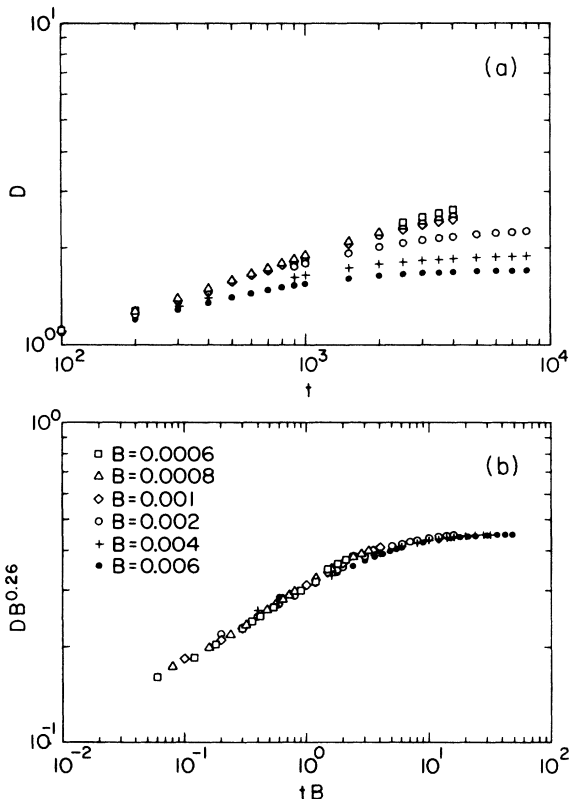


FIG. 10. The time evolution of the lamellar thickness  $D$  (a) plotted directly and (b) scaled according to (5.2). The data represents the average over five  $500 \times 500$  systems. The same result could be obtained from only one system, since  $D$  is determined locally.

Chakrabarti, Toral, and Gunton<sup>41</sup> have recently performed a Monte Carlo simulation of a BCP system and, relying on our argument that  $N^2 \sim t$ , have scaled the scattering function as

$$S(k, B) = D^2(B) F(kD(B)) \quad (5.3)$$

in two dimensions. They claim that their Monte Carlo model and our CDS model or its PDE counterpart are in the same universality class. It should be noted, however, that their system is rather dilute with the monomer density far less than the BCP melt.

A more explicit discussion of the exponent equality for the SS regime is as follows. Although the true equilibrium parallel stripe patterns require global transport of polymers as we have discussed above, the width of the pattern is determined by local rearrangements of polymers. That is, the lamellar thickness is determined by the local minima of the system free energy. The local minima can be efficiently searched by local dynamics, which is driven by the interface curvature. Thus the lamellar width is essentially determined by this dynamics. Therefore following Allen and Cahn,<sup>42</sup> we can reduce the problem to the study of the interface dynamics.<sup>43,2,13</sup> Defining a local coordinate  $n$  perpendicular to the interface and integrating the equation of motion for  $\psi$ , we get

$$\int dn \int da' G(\mathbf{r}(\mathbf{a}, n), \mathbf{r}_i(\mathbf{a}', t)) v(\mathbf{r}_i(\mathbf{a}', t)) + \frac{1}{2\psi_0} B \int dn \int d\mathbf{r}' G(\mathbf{r}, \mathbf{r}') \psi(\mathbf{r}', t) \propto K(\mathbf{r}_i(\mathbf{a}, t)), \quad (5.4)$$

where  $\mathbf{a}$  collectively denotes the coordinates along the interface,  $K$  is essentially the mean curvature of the interface, and  $\psi_0$  is the modulus of the equilibrium value of the order parameter far away from the interface. Let us assume that there is only one relevant length scale  $l$ . A simple dimensional analysis gives us  $[da] = [l]^{d-1}$ ,  $[G] = [l]^{2-d}$ ,  $[v] = [l]/[t]$ ,  $[K] = [l]^{-1}$ , and  $[dn] = 1$ . Hence we can reduce (5.4) to the following formal relation:

$$\frac{[l]^2}{[t]} + \frac{[l]^2}{[N^2]} = \frac{1}{[l]}. \quad (5.5)$$

Notice that the terms on the left-hand side of the formal equation (5.5) do not occur at the same time. For ordinary spinodal decomposition the second term is absent since  $B=0$  in this case, and we obtain  $l \sim t^{1/3}$ , as found by Kawasaki and Ohta.<sup>43</sup> For BCP microphase separation in local equilibrium, on the other hand, we do not have the first term which originates from the interface displacement. Consequently, we find that  $l \sim N^{2/3}$  in agreement with experimental results. Actually,  $\frac{2}{3}$  is twice the growth exponent for the spinodal decomposition.

The derivation of  $2\phi = \theta$  is legitimate, if the interface structure in a spinodally decomposing system and a BCP system are similar, even if the thin interface condition is not satisfied. Dimensionally, when the interface thickness is significant and the surface diffusion dominates the coarsening process,  $l(t) \sim t^{1/4}$  is expected for spinodal decomposition.<sup>44</sup> This regime corresponds to

the WS regime for BCP's, in which  $\theta = \frac{1}{2}$  as expected from the exponent equality.

## VI. EXACT RESULTS

Ohta and Kawasaki's variational computation of the lamellar thickness exponent<sup>25</sup> strongly suggests that the dimensional analysis is actually exact. We would like to demonstrate that this is indeed the case with an exactly solvable model of BCP. To this end we exploit the universality property that the global features of the model is not dependent on the details of the model. We know from our experience with spinodal decomposition that the details of the free energy functional are irrelevant. The choice of the map  $f$  in (3.2) is not important as long as it satisfies the conditions mentioned before. This is the main reason why our gross modeling of spinodal decomposition can give realistic results. Although this is an empirical fact supported by computational results with the aid of CDS, it is not hard to understand this universality intuitively. The details of the functional form of the free energy affect the interface only. The interface structure, on the other hand, affects the actual values of surface tension, which may alter the time scale of the pattern evolution, but not the coarsening mechanism. Hence, the detail of the interface structure is unimportant.

We can exploit this fact to invent a potential function which allows an analytical solution for the lamellar density profile. We found the following potential convenient:<sup>14</sup>

$$\Phi(\psi) = \frac{1}{2}[\psi - \text{sgn}(\psi)]^2. \quad (6.1)$$

This gives the correct local flow diagram, although it is not differentiable at the origin. This causes a pathologi-

cal behavior for the WS regime, which is not our concern. With this local free-energy function the cross-sectional density profile of the lamellar structure in the steady state obeys the following linear ordinary differential equation, which is just (5.1):

$$\frac{d^2\psi}{dx^2} - \frac{d^4\psi}{dx^4} = B\psi. \quad (6.2)$$

The boundary condition at the interface where  $\psi=0$  is the twice differentiability of the driving force:  $\psi - \text{sgn}(\psi) - d^2\psi/dx^2$ .

It is easy to find the general periodic solution which gives a symmetric density profile for each lamella. It reads

$$\psi(x) = \frac{1}{\sqrt{1-4B}} \left[ \frac{\cosh\beta x}{\cosh\beta D/2} - \frac{\cosh\alpha x}{\cosh\alpha D/2} \right], \quad x \in [-D/2, D/2], \quad (6.3)$$

where  $\alpha = [(1 + \sqrt{1-4B})/2]^{1/2}$  and  $\beta = [(1 - \sqrt{1-4B})/2]^{1/2}$ . This contains one free parameter, the thickness  $D$ . Since we are looking for the equilibrium lamellar thickness, the profile must minimize the free-energy density. We can compute the free-energy density for the periodic profile given by (6.3) as (cf. Ref. 27)

$$F(D) = \frac{1}{2D} \int_0^{D/2} dx \left[ \left( \frac{d\psi}{dx} \right)^2 + (\psi - 1)^2 \right] - \frac{B}{2D} \int_0^{D/2} dx \int_0^x dy (x - D) \psi(x) \psi(y). \quad (6.4)$$

Thus the full analytic formula for the free energy is given by

$$\begin{aligned} \gamma^2 DF = & \frac{D}{4} (\alpha^2 - 1) \tanh^2 \left[ \frac{\alpha D}{2} \right] + \tanh \left[ \frac{\alpha D}{2} \right] \left[ \frac{\alpha}{2} - \frac{2\alpha(\alpha\beta + 1)}{\gamma} + \frac{1 + 4\alpha}{2\alpha} \right] \\ & + \frac{D}{4} (\beta^2 - 1) \tanh^2 \left[ \frac{\beta D}{2} \right] + \tanh \left[ \frac{\beta D}{2} \right] \left[ \frac{\beta}{2} + \frac{2\beta(\alpha\beta + 1)}{\gamma} + \frac{1 + 4\beta}{2\beta} \right] \\ & - 2B \left[ \frac{D}{8\beta^2} - \frac{D \tanh^2(\beta D/2)}{8\beta^2} - \frac{\tanh(\beta D/2)}{4\beta^3} + \frac{\tanh(\beta D/2)}{\beta\gamma} \right. \\ & \left. + \frac{D}{8\alpha^2} - \frac{D \tanh^2(\alpha D/2)}{8\alpha^2} - \frac{\tanh(\alpha D/2)}{4\alpha^3} + \frac{\tanh(\alpha D/2)}{\alpha\gamma} \right], \quad (6.5) \end{aligned}$$

where  $\gamma = \sqrt{1-4B}$ . This free energy is holomorphic in  $\sqrt{B}$  near the origin. For the small- $B$  parameter, this can be expanded as

$$\begin{aligned} \sqrt{1-4B} F(D) = & \frac{\tanh(D/2)}{D} - 2\sqrt{B} \frac{\tanh(D/2)}{D} \\ & + B \left[ \frac{D^2}{24} - \frac{2}{\cosh^2(D/2)} - \frac{19 \tanh(D/2)}{D} \right. \\ & \left. - \frac{\tanh^2(D/2)}{2} + \dots \right]. \quad (6.6) \end{aligned}$$

Minimization of the above expansion gives  $D \sim B^{-1/3}$  for sufficiently large  $D$ . Comparing (6.6) and (5.5), we may conclude that the dimensional analytical result is not fortuitous. The density profile is shown in Fig. 11. It should be noted that the density maxima occur near the phase boundaries. This was already found by Liu<sup>27</sup> numerically.

We can compute the  $B$ - $D$  relation numerically using the full expression (6.5) for the free energy as a function of  $D$ . The result is in Fig. 12. This is quite different from the result due to Liu and Goldenfeld;<sup>27</sup> in their case, a smooth crossover to the WS regime was found. The

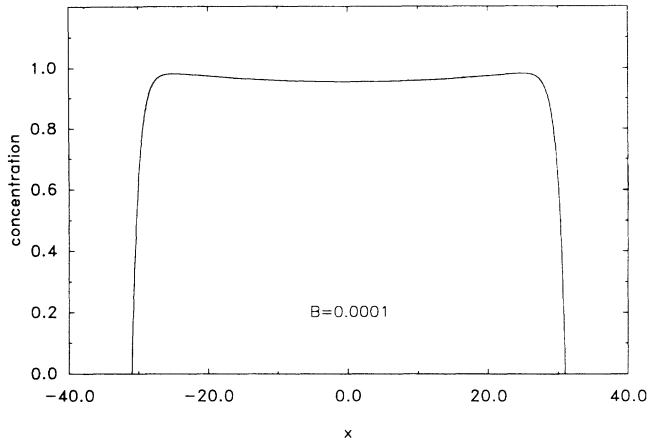


FIG. 11. Cross-sectional density profile of a lamella given by (6.6) with the equilibrium thickness.

pathological behavior of our model is solely due to the nondifferentiability of the potential at the origin. For the WS regime it is crucial that the square gradient term in the free-energy density dominates the contribution of the term  $\Phi$ . This is possible only when the contribution from  $\Phi$  is negligible at least qualitatively. For this to be true  $\Phi$  must have a differentiable maximum near the origin. In our case  $\Phi$  is of order  $\psi$  near the origin, so that, for smaller amplitudes of  $\psi$ ,  $\Phi$  dominates the free-energy density, and the WS exponent for our model becomes larger than  $\frac{1}{2}$ . Incidentally, the potential we adopted allows exact closed solutions describing droplets when  $B=0$ .

## VII. DISCUSSION

We have discussed a mesoscale model of block-copolymer microphase separation dynamics based on our cell-dynamics-system model, and the partial differential equations suggested by the former. Even with our computationally efficient modeling scheme, we could not go into the strong segregation regime. We need a better modeling technique than CDS to this end. Although our CDS model is not computationally efficient enough, the CDS modeling method based on the philosophy of pursuing the mathematical simplicity has suggested a physically sounder model than the existing mesoscale models derived from more microscopic models as discussed in detail in Sec. III. Furthermore, the partial-differential-equation version of our model has clearly demonstrated a close relation between the problem of BCP lamellar thickness and binary alloy spinodal decomposition. This has led us to conclude that there is a simple relation be-

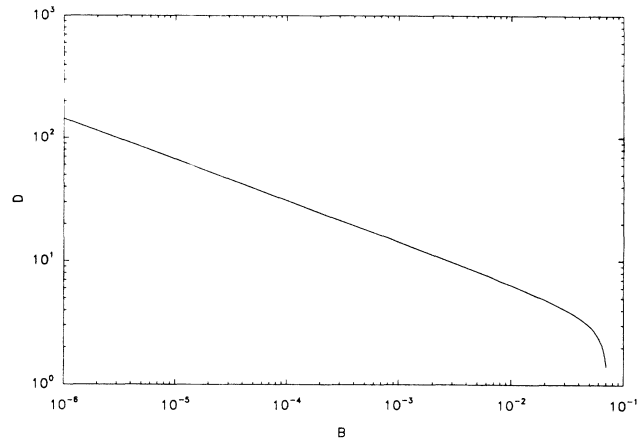


FIG. 12. Relation between  $B$  and the equilibrium domain size  $D$  resulting from the minimization of the free energy (6.5). The line has the slope  $\frac{1}{3}$  for  $B \leq 10^{-3}$ .

tween the exponents in each problem. An analytically solvable version of the PDE model exactly gives the lamellar thickness exponent in the SS regime.

We have pointed out the crucial importance of fluidity to get globally ordered patterns. By adding solvent to the system, and adjusting the temperature, it should be possible to study systematically the effect of fluidity on the time evolution of mesoscale patterns. This experiment could be done in two dimensions by sandwiching a BCP-solvent mixture between two plates (i.e., in the Hele-Shaw cell) as is demonstrated numerically in Sec. III. Although the hydrodynamics in the Hele-Shaw cell is quite different from the bulk hydrodynamics, the fluidity is not spoiled. Spinodal decomposition of binary fluids in the Hele-Shaw cell demonstrates drastic effects on the time scale of the coarsening process.<sup>11</sup> More detailed study on the effect of flow will be discussed elsewhere.

## ACKNOWLEDGMENTS

The authors are grateful to Ari Shinozaki for the discussion of hydrodynamic effects and for critically reading the manuscript. Very helpful discussions with Nigel Goldenfeld, Fong Liu, and Takao Ohta are gratefully acknowledged. This work is, in part, supported by the National Science Foundation Grant Nos. DMR 87-01393 and DMR 86-12860 (through University of Illinois, Materials Research Laboratory), by Coordenação de Aperfeiçoamento de Pessoal de Nível Superior (Brazil) and by a grant from Cray Research Inc. for usage of the National Center for Supercomputing Applications CRAY X-MP 48 computer.

<sup>1</sup>Y. Oono and S. Puri, Phys. Rev. Lett. **58**, 836 (1987).

<sup>2</sup>Y. Oono and S. Puri, Phys. Rev. A **38**, 434 (1988); S. Puri and Y. Oono, *ibid.* **38**, 1542 (1988).

<sup>3</sup>Y. Oono and A. Shinozaki, Forma (to be published).

<sup>4</sup>T. Ohta, Y. Enomoto, K. Kawasaki, and A. Sato, in *Dynamics of Ordering Processes in Condensed Matter*, edited by S. Komura and H. Furukawa (Plenum, New York, 1988).

<sup>5</sup>Y. Oono and Y. Shiwa, Mod. Phys. Lett. B **1**, 49 (1987).

- <sup>6</sup>A. Chakrabarti and J. D. Gunton, *Phys. Rev. B* **37**, 3798 (1988).
- <sup>7</sup>M. Mondello and N. Goldenfeld (unpublished).
- <sup>8</sup>Y. Oono, S. Puri, C. Yeung, and M. Bahiana, *J. Appl. Crystallogr.* **21**, 883 (1988).
- <sup>9</sup>H. Furukawa, *Phys. Rev. B* **40**, 2341 (1989).
- <sup>10</sup>C. Yeung, *Phys. Rev. Lett.* **61**, 1135 (1988).
- <sup>11</sup>A. Shinozaki and Y. Oono (unpublished).
- <sup>12</sup>L. Leibler, *Macromolecules* **13**, 1602 (1980).
- <sup>13</sup>Y. Oono and M. Bahiana, *Phys. Rev. Lett.* **61**, 1109 (1988).
- <sup>14</sup>Y. Oono and M. Bahiana, *J. Phys.: Condens. Matter* **1**, 5297 (1989).
- <sup>15</sup>T. Inoue, T. Soen, T. Hashimoto, and H. Kawai, *Macromolecules* **7**, 1283 (1969).
- <sup>16</sup>H. Hasegawa, H. Tanaka, K. Yamasaki, and T. Hashimoto, *Macromolecules* **20**, 1651 (1987).
- <sup>17</sup>G. Kämpf, M. Hoffman, and H. Krömer, *Ber. Bunsenges, Phys. Chem.* **74**, 851 (1970).
- <sup>18</sup>A. Douy and B. R. Gollot, *Mol. Cryst. Liquid Cryst.* **14**, 191 (1971).
- <sup>19</sup>T. Hashimoto, M. Shibayama, and H. Kawai, *Macromolecules* **13**, 1237 (1980).
- <sup>20</sup>D. J. Meier, *J. Polym. Sci., Part C* **26**, 81 (1969).
- <sup>21</sup>E. Helfand, *Macromolecules* **8**, 552 (1975).
- <sup>22</sup>E. Helfand and Z. R. Wasserman, *Macromolecules* **9**, 879 (1976).
- <sup>23</sup>E. Helfand and Z. R. Wasserman, *Macromolecules* **11**, 960 (1978).
- <sup>24</sup>E. Helfand and Z. R. Wasserman, *Macromolecules* **13**, 994 (1980).
- <sup>25</sup>T. Ohta and K. Kawasaki, *Macromolecules* **19**, 2621 (1986). See also Ref. 26.
- <sup>26</sup>K. Kawasaki, T. Ohta, and M. Kohroghi, *Macromolecules* **21**, 2972 (1989).
- <sup>27</sup>F. Liu and N. Goldenfeld, *Phys. Rev. A* **39**, 4805 (1989).
- <sup>28</sup>M. Olvera de la Cruz, *J. Chem. Phys.* **90**, 1995 (1989).
- <sup>29</sup>E. Di Marzio, *Macromolecules* **21**, 2262 (1989).
- <sup>30</sup>A. Chakrabarti, R. Toral, and J. D. Gunton, *Phys. Rev. B* **39**, 4386 (1989).
- <sup>31</sup>S. Puri and Y. Oono, *J. Phys. A* **21**, L755 (1988).
- <sup>32</sup>K. Kawasaki and T. Ohta (unpublished).
- <sup>33</sup>S. F. Edwards, *Proc. Phys. Soc. London* **88**, 265 (1966).
- <sup>34</sup>T. Ohta and Y. Oono, *Phys. Lett.* **89A**, 460 (1982).
- <sup>35</sup>J. W. Cahn and J. H. Hilliard, *J. Chem. Phys.* **28**, 258 (1958).
- <sup>36</sup>Y. Higuchi, *Colloq. Math. Janos Bolyai* **27**, 517 (1979).
- <sup>37</sup>M. Aizenmann, *Commun. Math. Phys.* **73**, 83 (1980).
- <sup>38</sup>R. L. Dobrushin, *Funct. Anal. Appl.* **2**, 292 (1968); **2**, 302 (1968).
- <sup>39</sup>Y. Rabin (private communication).
- <sup>40</sup>K. Kawasaki and T. Ohta, *Physica A* **118**, 175 (1983); K. Kawasaki, *Butsuri* **38**, 919 (1983).
- <sup>41</sup>A. Chakrabarti, R. Toral, and J. D. Gunton, *Phys. Rev. Lett.* **63**, 2661 (1989).
- <sup>42</sup>S. M. Allen and J. W. Cahn, *Acta Metall.* **27**, 1085 (1979).
- <sup>43</sup>K. Kawasaki and T. Ohta, *Prog. Theor. Phys.* **67**, 147 (1982); *Physica A* **118**, 175 (1983).
- <sup>44</sup>H. Furukawa, *Adv. Phys.* **34**, 703 (1985).

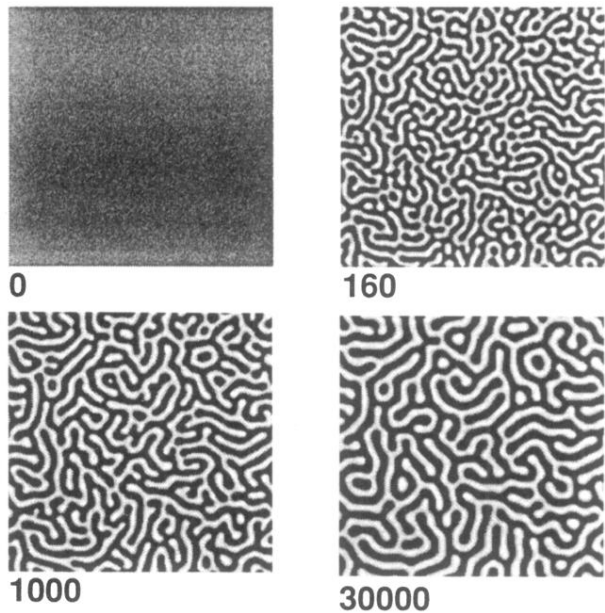


FIG. 2.  $200 \times 200$  patterns with  $A = 1.3$ ,  $\mathcal{D} = 0.5$ ,  $B = 0.005$ ,  $r = \frac{1}{2}$ . The numbers denote time steps. The pattern does not change significantly after about 10 000 steps.

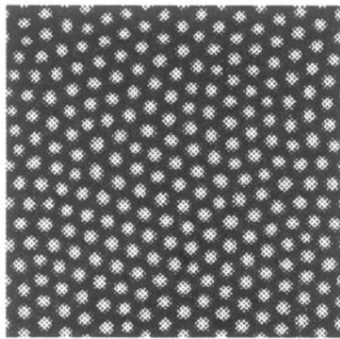


FIG. 3.  $128 \times 128$  pattern after 30 000 iterations with  $A = 1.3$ ,  $\mathcal{D} = 0.5$ ,  $B = 0.02$ , and  $r = 0.4$ .

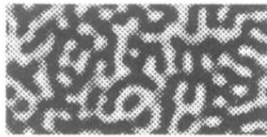


FIG. 4. Cross section of a 3D system with the lattice size  $100 \times 100 \times 50$  with  $A = 1.3$ ,  $\mathcal{D} = 0.5$ , and  $B = 0.02$  at  $t = 1000$ .

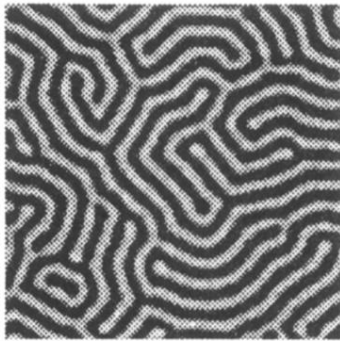


FIG. 5. Pattern after 30 000 steps obtained from (3.4) with noise added in the following way:

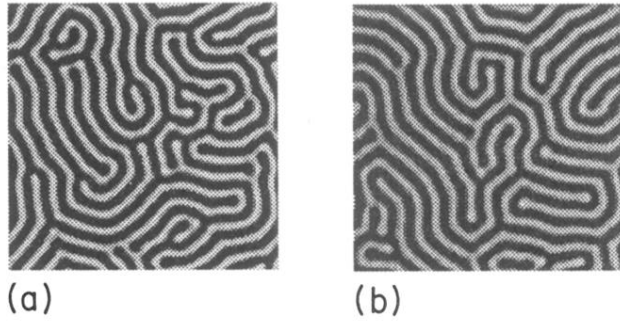


FIG. 6. Effect of the penalty for the interface bending after 30 000 timesteps. The patterns are  $128 \times 128$  and have  $A = 1.3$ ,  $\mathcal{D} = 0.45$ , and  $B = 0.02$ . In (a)  $b = 0$ , that is, no penalty. In (b)  $b = 1.1$ . Both patterns were obtained starting from the same initial condition.

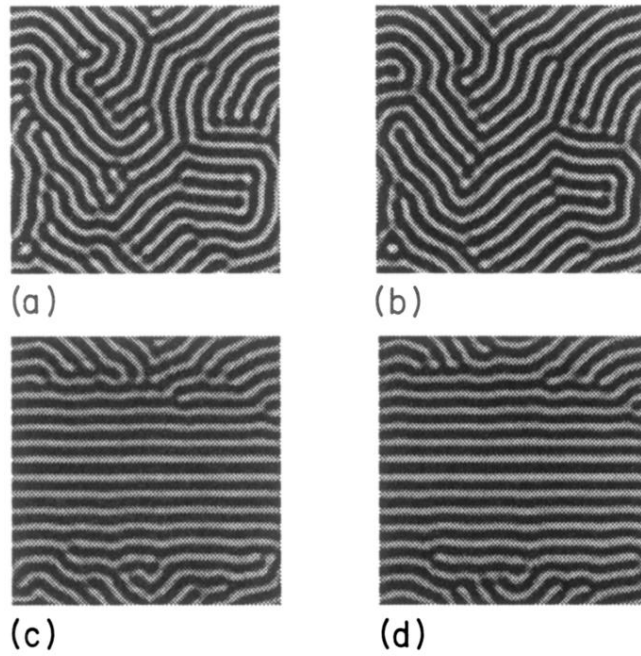


FIG. 7. Effect of the boundary conditions in the formation of lamella. Patterns on the left correspond to 10 000 iterations, and on the right, 30 000. Here,  $A = 1.22$  and  $B = 0.02$ . (a) and (b) have periodic boundary conditions in both directions; (c) and (d) have the central line fixed at  $\psi = 0.5$ . The introduction of a fixed boundary condition has promoted some ordering, but the evolution of the pattern after 10 000 iterations is extremely slow. Layers with large component parallel to ordering direction are almost frozen.

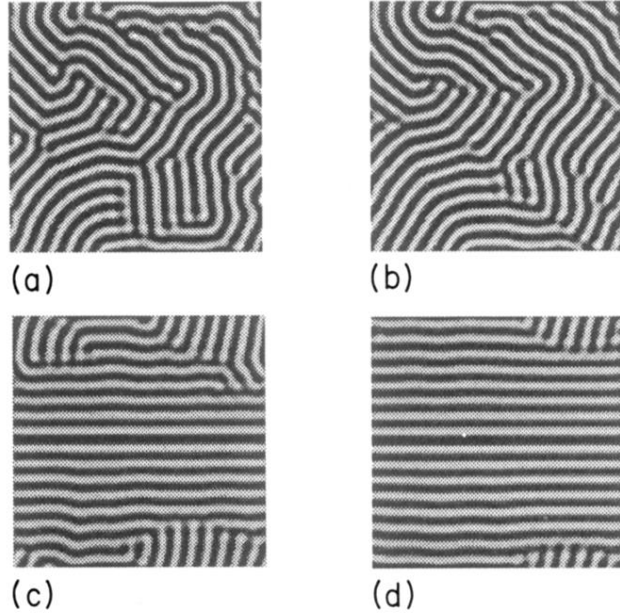


FIG. 8. Effect of hydrodynamic interactions in the formation of lamellar patterns, in a Hele-Shaw cell. To incorporate global flow in our model, we followed Shinozaki and Oono (Ref. 11). A term corresponding to the fluid motion was added to (3.5). Assuming the incompressibility condition for the velocity field  $\nabla \cdot \mathbf{v} = 0$  the resulting equation is  $\partial\psi/\partial t = \Delta(\delta H/\delta\psi) - \mathbf{v} \cdot \nabla\psi$ .  $\mathbf{v}$  can be calculated starting from the Navier-Stokes equation with the introduction of the following approximations: (i) the fluid is considered to be in the Stokes regime; (ii) the velocity field is slaved to the slower process of phase separation; (iii) the distance between the planes in the Hele-Shaw cell is much smaller than the domain size, so that we can eliminate  $\Delta$  in favor of a geometric factor  $-c^2$ , which is roughly the inverse of the interplate distance squared. With these we get  $\mathbf{v} = -1/c^2 \nu [\nabla p + \psi \nabla(\delta H/\delta\psi)]$ , where  $p$  is the pressure and  $\nu$  the kinematic viscosity.  $-\psi \nabla \delta H/\delta\psi$  is a force density felt by the fluid due to the existence of a chemical “pressure”  $\delta H/\delta\psi$ . The incompressibility constraint allows us to compute the pressure, and hence the velocity field. A  $128 \times 128$  lattice is used with  $A = 1.22$ ,  $D = 0.45$ ,  $\nu c^2 = 2.0$ ,  $B = 0.02$ . The patterns on the left correspond to 10 000 timesteps, and on the right, 30 000. The systems in (a) and (b) have periodic boundary conditions in both directions. (c) and (d) have the central line fixed at  $\psi = 0.5$ . We can see that the fixed boundary condition is essential for obtaining a well structured lamellar pattern. The ordered lamella are formed from domains oriented perpendicularly to the fixed surface, a condition that appears only when flow is added to the simulation (compare with Fig. 7). Also it is important to notice that although the equilibrium lamellar size is well established before  $t = 5000$  time steps for this value of  $B$ ; only after 30 000 iterations is the ordered pattern obtained.